Seasonal cycle of O_2 and pCO_2 in the central Labrador Sea: Atmospheric, biological, and physical implications

A. Körtzinger,[1] U. Send,[2] D. W. R. Wallace,[1] J. Karstensen,[3] and M. DeGrandpre[4]

Received 4 June 2007; revised 12 October 2007; accepted 9 November 2007; published 14 February 2008.

[1] We present full 2004–2005 seasonal cycles of CO_2 partial pressure (pCO_2) and dissolved oxygen (O_2) in surface waters at a time series site in the central Labrador Sea (56.5°N, 52.6°W) and use these data to calculate annual net air-sea fluxes of CO_2 and O_2 as well as atmospheric potential oxygen (APO). The region is characterized by a net CO_2 sink (2.7 ± 0.8 mol CO_2 m^{-2} yr^{-1}) that is mediated to a major extent by biological carbon drawdown during spring/summer. During wintertime, surface waters approach equilibrium with atmospheric CO_2. Oxygen changes from marked undersaturation of about 6% during wintertime to strong supersaturation by up to 10% during the spring/summer bloom. Overall, the central Labrador Sea acts as an O_2 sink of 10.0 ± 3.1 mol m^{-2} yr^{-1}. The combined CO_2 and O_2 sink functions give rise to a sizable APO flux of 13.0 ± 4.0 mol m^{-2} yr^{-1} into surface waters of the central Labrador Sea. A mixed layer carbon budget yields a net community production of 4.0 ± 0.8 mol C m^{-2} during the 2005 productive season about one third of which appears to undergo subsurface respiration in a depth range that is reventilated during the following winter. The timing of the spring bloom is discussed and eddies from the West Greenland Current are thought to be associated with the triggering of the bloom. Finally, we use CO_2 and O_2 mixed layer dynamics during the 2005 spring bloom to evaluate a suite of prominent wind speed-dependent parameterizations for the gas transfer coefficient. We find very good agreement with those parameterizations which yield higher transfer coefficients at wind speeds above 10 m s^{-1}.

Citation: Körtzinger, A., U. Send, D. W. R. Wallace, J. Kartensen, and M. DeGrandpre (2008), Seasonal cycle of O_2 and pCO_2 in the central Labrador Sea: Atmospheric, biological, and physical implications, *Global Biogeochem. Cycles*, *22*, GB1014, doi:10.1029/2007GB003029.

1. Introduction

[2] The subpolar North Atlantic is characterized by large seasonal amplitudes of surface ocean carbon and oxygen dynamics and associated source/sink functions for atmospheric CO_2 and O_2 [*Najjar and Keeling*, 1997; *Garcia and Keeling*, 2001; *Takahashi et al.*, 2002]. Key to this dynamic behavior is the combination of both strong physical and biological forcing of the subpolar gyre in the North Atlantic. The Labrador Sea is a region of particular interest, being one of the few regions of the world ocean where open ocean deep convection occurs, reaching depths between 700 and more than 2000 m [*Lazier et al.*, 2002; *Avsic et al.*, 2006]. The Labrador Sea is part of the Atlantic Arctic Province (ARCT) of *Longhurst* [2007] which is characterized by large "spring bloom type" biological productivity in May–June fueled by vertical nutrient supply during winter convection. Seasonal variations of both physical factors (warming/cooling, deep convection and entrainment, wind speed etc.) and biological factors (productivity/respiration) drive air-sea exchanges of CO_2 and O_2. This seasonal forcing of gas exchange (e.g., warming simultaneous with primary production) is reinforcing in the case of O_2 exchange and self-compensating for CO_2. This complex forcing and high-amplitude seasonal variability coupled with the direct link to the vast ocean interior makes the region interesting, significant, and potentially vulnerable in the anthropocene era of global climate change.

[3] All major forcing factors (temperature [*Levitus et al.*, 2005], salinity [*Dickson et al.*, 2002], convection depth [*Lazier et al.*, 2002; *Avsic et al.*, 2006], and biological productivity [*Behrenfeld et al.*, 2006]) are affected by subdecadal variability as well as longer-term climate-driven trends. These changes are bound to influence the CO_2 sink in the subpolar North Atlantic and may exert a significant control on the growth rate of CO_2 in the atmosphere as well as on our future climate. Temporal variability in the degree of surface seawater CO_2 saturation, and hence the

[1]Leibniz Institute of Marine Sciences, Chemical Oceanography, University of Kiel, Kiel, Germany.
[2]Scripps Institution of Oceanography, University of California at San Diego, La Jolla, California, USA.
[3]Leibniz Institute of Marine Sciences, Physical Oceanography, University of Kiel, Kiel, Germany.
[4]Department of Chemistry, University of Montana, Missoula, Montana, USA.

0886-6236/08/2007GB003029$12.00

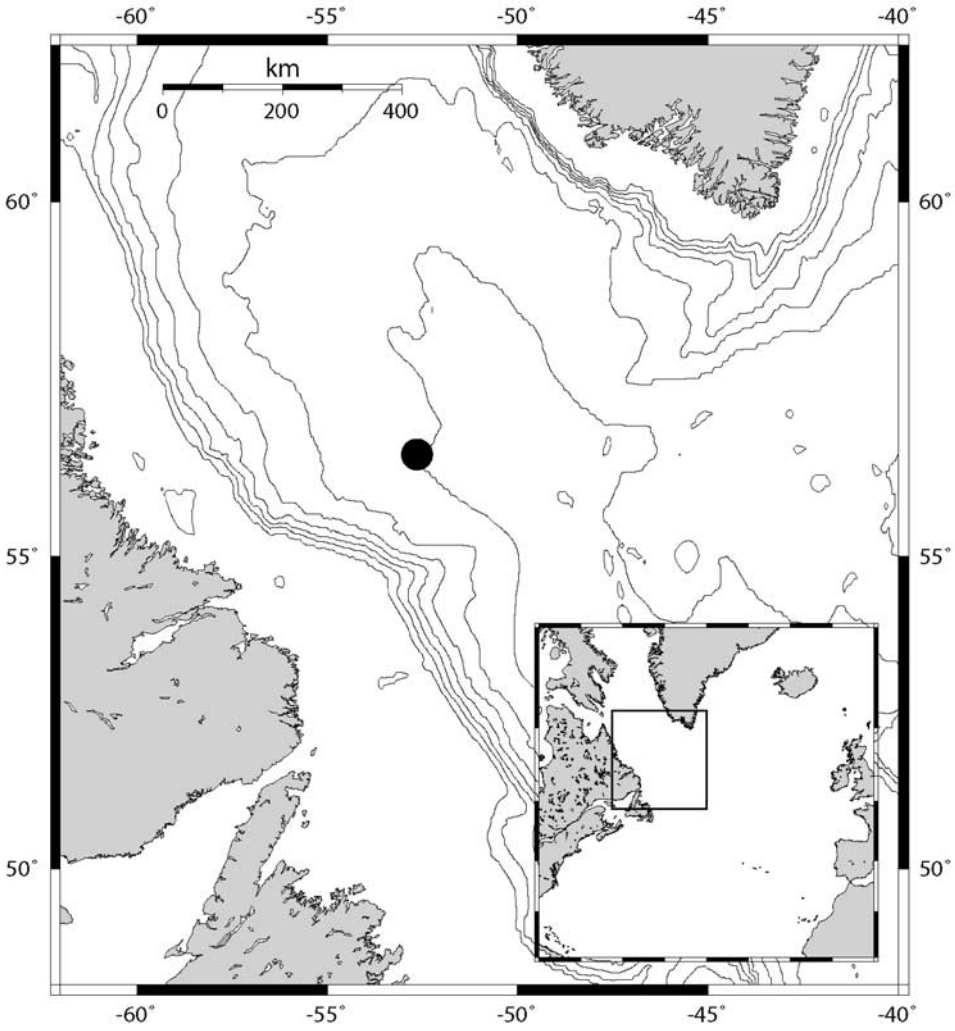

Figure 1. Map of the Labrador Sea in the subpolar northwest Atlantic Ocean with the location of the K1 mooring site at 56.5°N, 52.5°W. The bathymetry contour interval is 500 m.

corresponding sink for atmospheric CO_2, is starting to be observed [e.g., *Lefèvre et al.*, 2004; *Omar and Olsen*, 2006]. Measurement of such variability and attribution to variable forcing is critical for testing and improving models (including models of air-sea gas exchange) used to predict or explain future changes in atmospheric CO_2 and O_2. The main emphasis of this study is on the application of in situ measurement technology to examine the seasonal CO_2 and O_2 variability in the surface water of the Labrador Sea.

2. Methods and Data

2.1. Central Labrador Sea Mooring (K1)

[4] Since 1996 a long-term oceanographic mooring site has been operated continuously in the subpolar northwest Atlantic Ocean at the K1 location in the central Labrador Sea (56.5°N, 52.6°W (Figure 1)). The site, which is close to the location of the former Ocean Weather Station Bravo (56.5°N, 51°W), was chosen primarily to study trends and variability in deep convection activity [*Avsic et al.*, 2006]. Following a pilot study that took place in 2001 [*DeGrandpre et al.*, 2006], continuous mixed layer measurements of O_2 concentration and CO_2 partial pressure (pCO_2) have been made with autonomous instrumentation deployed at the K1 site from September 2004 to July 2005. Therein pCO_2 and O_2 sensors as well as a CTD sensor were deployed together at a nominal depth of about 38 m. Since the mooring featured a subsurface top flotation element instead of a surface buoy this was the closest the instrument package could be deployed to the surface, which has implications for the observability of mixed layer properties (see section 3.1).

2.2. Measurements

[5] A suite of physical (temperature, salinity, and pressure) and chemical parameters (pCO_2 and O_2) were measured successfully with autonomous instrumentation deployed at various depths at K1 (Table 1). Following is a brief description of the instrument used: The pCO_2 was

Table 1. Nominal Deployment Depths (Sampling Intervals) of Moored Instruments From Which Data Have Been Used in This Study

Parameter	Deployment Depths (Sampling Interval)
Temperature[a]	38 m, 92 m, 156 m, 246 m, 305 m, 422 m, 798 m (12 hour)
Salinity[a]	38 m, 92 m, 246 m, 798 m (12 hour)
Pressure	38 m, 92 m, 156 m, 246 m, 422 m, 798 m (12 hour)
Oxygen	38 m, 798 m (2 hour)
pCO_2	38 m (1 hour)

[a] *T/S* sensor at 10-m depth lost after a few days into the deployment.

measured with an autonomous sensor (SAMI-CO_2, Sunburst Sensors LLC, Missoula, Montana, United States) which is based on equilibration of a pH indicator solution contained in a gas permeable membrane with ambient pCO_2 and subsequent spectrophotometric pH determination in the equilibrated solution [*DeGrandpre et al.*, 1995]. The sensor head was covered with a copper mesh to prevent biofouling. Oxygen measurements were made with a novel optode sensor (Model 3830, Aanderaa Data Instruments, Bergen, Norway) which senses O_2 partial pressure via its quenching effect on the fluorescence of a dye immobilized in a gas permeable sensing foil. This sensor has shown very good sensitivity and long-term stability [*Körtzinger et al.*, 2005; *Tengberg et al.*, 2006]. Measurements of temperature, salinity, and pressure were performed with SBE-37 MicroCAT recorders (Sea-Bird Electronics Inc., Bellevue, Washington, United States) and at some depths with RCM-8 current meters equipped with temperature sensors only (Aanderaa Data Instruments, Bergen, Norway).

2.3. Sources of Ancillary Data

[6] In the present analysis we made use of various other sources of information (Table 2) for the following parameters: sea surface temperature (SST), sea level barometric pressure (SLP), wind speed at 10 m height, atmospheric CO_2 concentration, climatological surface ocean pCO_2, and total alkalinity (A_T). Data were retrieved for the pixel (or average of pixels) that represents the location of the K1 site (56.5°N, 52.6°W).

[7] We used the extended CO_2 record derived from continuous measurements on Vestmannaeyjar, Iceland (ICE (63.25°N, 20.15°W)) to calculate atmospheric pCO_2 at barometric pressure (28-day running mean of SLP taken every 6 hours, Table 2) and 100% humidity (derived from 28-day running mean of Advanced Microwave Scanning Radiometer-EOS (AMSR-E) SST, Table 2).

[8] Climatological surface ocean pCO_2 data were retrieved for the K1 site from *Takahashi et al.*'s [2002] climatology. As the climatology's reference year is 1995, a correction to our 2004–2005 observation period was necessary. For this the increase of the annual mean atmospheric CO_2 mole fraction at the Mace Head Observatory relative to 1995 was added to the 1995 climatological pCO_2 for the K1 site pixel. This correction assumes that the ocean follows the atmospheric CO_2 increase with an air-sea disequilibrium that is not changing with time. In reality this may not be exactly the case, but the currently available information does not provide a quantitatively consistent picture for an alternative correction.

[9] Mixed layer depths were estimated from vertical temperature, salinity, and (if available) oxygen profiles measured by Argo floats within ~100 km of the K1 site. Because of the region's weak vertical stratification during wintertime, classical mixed layer depth criteria such as the temperature ($\Delta T = 0.5$°C) or density criterion ($\Delta\sigma = 0.125$ kg m^{-3}) of *Monterey and Levitus* [1997] were not applicable. Weak vertical temperature and salinity gradients during periods of deeper mixing caused a strong overestimation of mixed layer depths using these criteria. Following *de Boyer Montégut et al.* [2004], we employed smaller but slightly variable criteria ($\Delta T \sim 0.2$°C and $\Delta\sigma \sim 0.03$ kg m^{-3}) on the basis of visual inspection of individual profiles. Where oxygen data were available, an oxygen criterion ($\Delta O_2 = 5$ μmol L^{-1}) was applied for an independent estimate. The three estimates agreed on average to within 6% (0–33%, larger relative differences only for shallow mixed layers) and we herein use averages of the three estimates.

2.4. Calibration of O_2 and pCO_2 Data

[10] The oxygen optodes are provided with batch-calibrated sensor foils. The nominal sensor accuracy stated by

Table 2. Sources of Ancillary Data Used in the Present Study

Parameter	Source
Sea surface temperature	Advanced Microwave Scanning Radiometer-EOS on NASA EOS Aqua satellite, level 3 daily product in 0.25° × 0.25° resolution [*Wentz and Meissner*, 2004]
Barometric pressure	Fleet Numerical Meteorology and Oceanography Center (FNMOC), sea level pressure on a 1° × 1° grid every 6 hours, Pacific Fisheries Environmental Laboratory (PFEL) live access server (http://www.pfeg.noaa.gov/products/las.html)
Vertical T/S profiles	Argo float observatory, Argo Global Data Assembly Centers, Global Ocean Data Assimilation Experiment (http://www.usgodae.org/cgi-bin/argo_select.pl)
10 m wind speed	FNMOC, sea level pressure on a 1° × 1° grid every 6 hours, PFEL live access server (http://www.pfeg.noaa.gov/products/las.html)
Atmospheric CO_2	GLOBALVIEW-CO_2 (2006). Cooperative Atmospheric Data Integration Project (http://www.esrl.noaa.gov/ccgg/globalview/)
Surface ocean pCO_2	Climatology for reference year 1995 [*Takahashi et al.*, 2002]
Surface ocean alkalinity	Global Surface Ocean Alkalinity Climatology, calculated using regional A_T relationships [*Lee et al.*, 2006] and monthly mean sea surface temperature/sea surface salinity fields from the World Ocean Atlas 2001 (http://cdiac.ornl.gov/oceans/Lee_Surface_Alk_Climatol.html)
Chlorophyll *a*	Moderate Resolution Imaging Spectroradiometer, level 3 standard chlorophyll product (http://oceancolor.gsfc.nasa.gov/)
Net primary production	Ocean Productivity website with VGPM and CBPM products (http://web.science.oregonstate.edu/ocean.productivity/index.php)

the manufacturer is 8 μmol L^{-1} or 5% whichever is greater. Results from field deployments have shown, however, that the stated accuracy is frequently not met when compared to oxygen data measured by classical Winkler titration [*Körtzinger et al.*, 2005]. Therefore a two-point laboratory calibration was carried out prior to deployment which allowed adjustment of the sensor's calibration coefficients. For this, two controlled O_2 concentrations were obtained, one in air and one in a zero-oxygen solution. When measuring in vapor-saturated air, the sensor reports O_2 concentrations as if submerged in freshwater equilibrated with air at the temperature of the measurement. The expected O_2 reading can then be calculated (at 100% humidity) using the dry air mole fraction of O_2 (0.20946), the temperature-dependent O_2 solubility in freshwater [*Benson and Krause*, 1984], and the barometric pressure at the time of the calibration. The zero-oxygen solution was prepared by addition of 5 g of sodium sulfite (Na_2SO_3) in 500 mL of water. The resulting accuracy of our O_2 measurements is estimated at 2 μmol L^{-1}.

[11] The SAMI-CO_2 sensor was calibrated by the manufacturer to the expected variability range in temperature and pCO_2 and should thus be calibration-free on the user side. Also, SAMI-CO_2 sensors have shown on various occasions to have good long-term stability [*DeGrandpre et al.*, 1995, 1999]. However, postcalibration of field data has sometimes turned out to be necessary to account for problems with the initial calibration (possibly due to changes occurring during sensor shipment) or from drift [*Körtzinger et al.*, 2008]. Postcalibration of the data was not possible for this study but several lines of evidence allow for plausibility checks on the data.

[12] First, underway pCO_2 measurements made onboard the research vessels used for deployment and recovery of the mooring were used. Of these the September 2004 data (R/V *Charles Darwin*, cruise 162b) are incorrect, probably due to undetected gas leakage in the equilibrator gas circuit and therefore cannot be used. The data from the recovery on 21 July 2005 (R/V *Thalassa*) are of good quality. Unfortunately, the SAMI pCO_2 sensor was sensing subsurface conditions during most of July as evidenced by the SST filter (described in section 3.1). Hence the surface pCO_2 and SST data of that cruise can only be used as plausibility check. Assuming a seasonal pCO_2 minimum associated with the SST maximum, mooring and ship-based pCO_2 agree reasonably well, however. Second, our pCO_2 measurements were compared to the climatological pCO_2 [*Takahashi et al.*, 2002] at this location, corrected to our measurement period (see section 2.3 for details) with a strikingly good agreement. Finally, a third line of evidence can be drawn from the fact that seawater pCO_2 levels approached the atmospheric pCO_2 in February 2005 and stayed very close to it for more than 3 months during which neither biological production nor warming/cooling were likely to have drawn it away from equilibrium. Seawater and atmosphere pCO_2 should thus have stayed at or near equilibrium which is what we observed with seawater pCO_2 (376.8 ± 3.1 μatm) and atmospheric pCO_2 (379.4 ± 2.5 μatm) being on average only 2.6 μatm apart. Taking all this information together, we estimate an overall accuracy of our pCO_2 data of 5–10 μatm.

3. Results and Discussion

3.1. Seasonal Cycles of Surface Ocean pCO_2 and O_2

[13] The main goal of our study was to characterize full annual cycles of surface ocean pCO_2 and O_2 in terms of their physical and biological forcing. This was partly impaired by submergence of the sensor package from its normal deployment depths of 38 m (Table 1) to depths of up to 100 m during certain periods and events. Attempts to measure surface waters in direct contact with the atmosphere were also compromised when the mixed layer depth approached or shoaled above the instrument's deployment depth during some summer periods. Some of the data acquired during these times were collected from below the mixed layer and cannot be used to infer atmosphere-ocean exchanges.

[14] In order to exclude these data a filter based on SST was developed. Remotely sensed microwave SST data (AMSR-E, Table 2), which have been shown to agree very well with sea surface temperatures down to 10-m depth [*Emery et al.*, 2006], were compared with in situ temperatures measured at the pCO_2 sensor depth. The pCO_2 data were considered representative of the surface mixed layer when the in situ temperature differed by less than 0.8°C from the SST measured by the satellite-borne microwave instrument (Figure 2). This temperature criterion was adjusted to allow for small measurement error, small-scale variability in mixed layer temperature, and scatter associated with the AMSR-E temperature data (sensitivity is 0.3 K for an integration time of 2.6 ms). The filter proved very effective and mainly eliminated data from periods of high stratification and shallow mixing during summer 2005.

[15] The resulting picture of the seasonal pCO_2 cycle in the central Labrador Sea (Figure 3) shows a late winter maximum and a pronounced summer minimum. This pattern is caused by the counteracting effects of seasonal warming and spring/summer biological activity (see also *DeGrandpre et al.* [2006]). As has been shown for other subpolar regions [e.g., *Takahashi et al.*, 1993, 2002; *Lüger et al.*, 2004], the pCO_2 spring/summer drawdown due to net community production, as fueled by wintertime nutrient supply through deep vertical mixing, strongly exceeds the tendency for pCO_2 to increase as a result of the seasonal warming. Mixed layer pCO_2 levels approach atmospheric pCO_2 at a time when SST has reached its annual minimum where it remains for more than 3 months. Deep convection (Figure 2) already reached its maximum by mid-February but remained strong after that. With respiration presumably being rather small during this cold period of deep convection neither physical nor biological forcing on the surface pCO_2 appears strong enough to pull it away from near-atmospheric equilibrium.

[16] The situation changes drastically with the appearance of spring phytoplankton in early May which is associated with a pCO_2 drawdown of almost 100 μatm. Our ship-based survey in July 2005 suggests that the seasonal pCO_2 minimum coincides with the SST maximum in July–August.

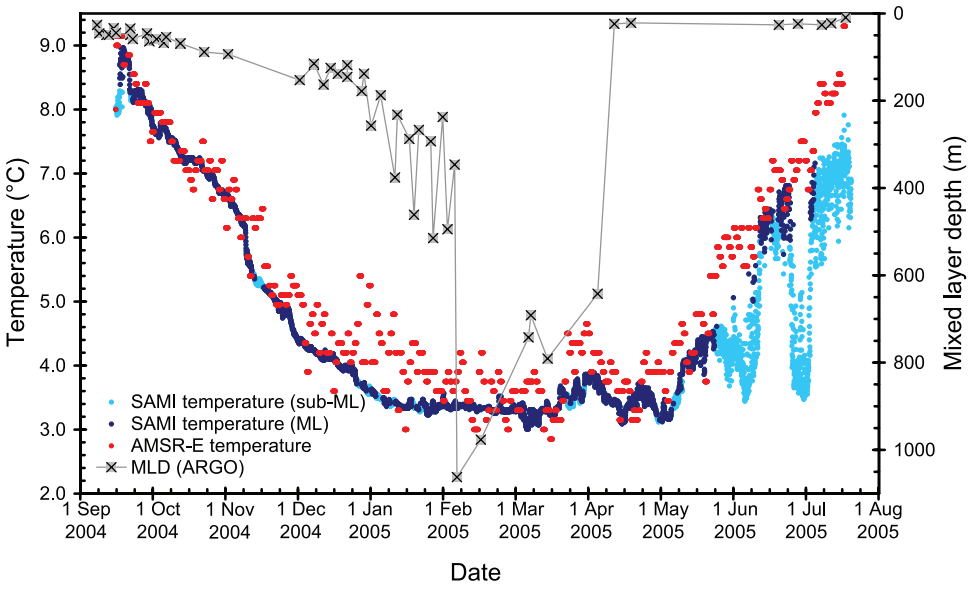

Figure 2. Comparison of temperature measurements made during the course of the K1 deployment by the SAMI pCO_2 sensor and the Advanced Microwave Scanning Radiometer-EOS on the NASA EOS satellite Aqua. The AMSR-E temperature data were used to distinguish mixed layer (ML) and submixed layer (sub-ML) location of the CO_2 sensor. Also shown is mixed layer depth estimated from Argo float profiles taken within ~100 km of the K1 mooring location.

After that, pCO_2 starts to rise continuously toward equilibrium despite the seasonal cooling. This cannot be explained by ongoing respiration and uptake of the atmospheric CO_2 alone, and we conclude that progressive deepening of the mixed layer entrains wintertime dissolved inorganic carbon (DIC) levels to the surface plus respiratory CO_2 that has been accumulating in shallow sub-surface depths since last deep convection. This return flux of CO_2 represents the fraction of

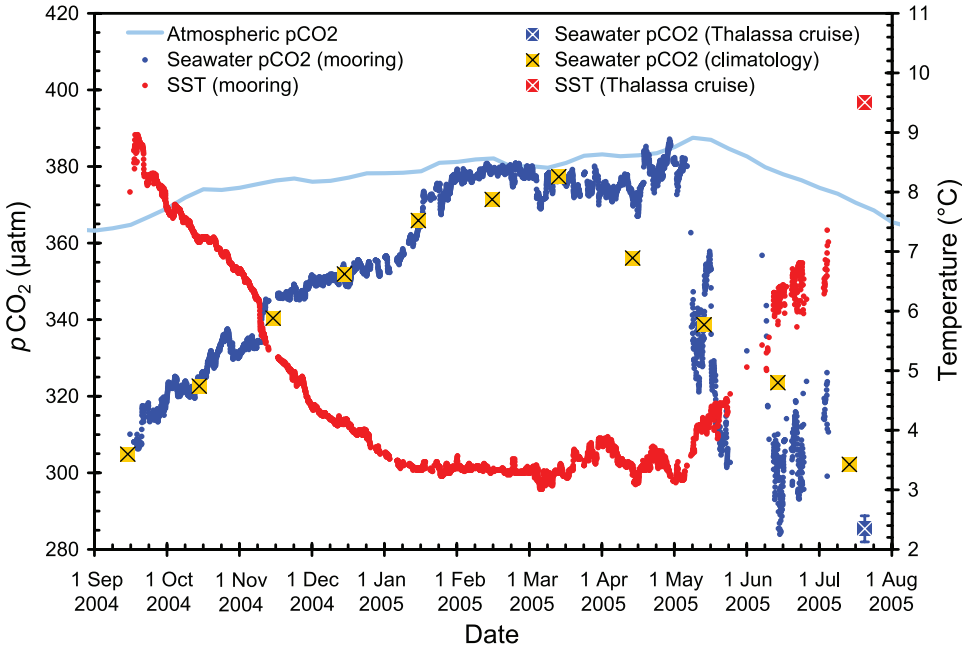

Figure 3. Mixed layer time series of pCO_2 and temperature measured during the course of the K1 deployment. For comparison, pCO_2 and temperature data from a ship-based survey in July 2005 are shown as is the climatological pCO_2 of *Takahashi et al.* [2002], corrected to the time and barometric pressure of the observational period. In addition, the atmospheric pCO_2 at barometric pressure is provided (from GLOBALVIEW-CO_2, 2006, ftp.cmdl.noaa.gov/ccg/co2/GLOBALVIEW).

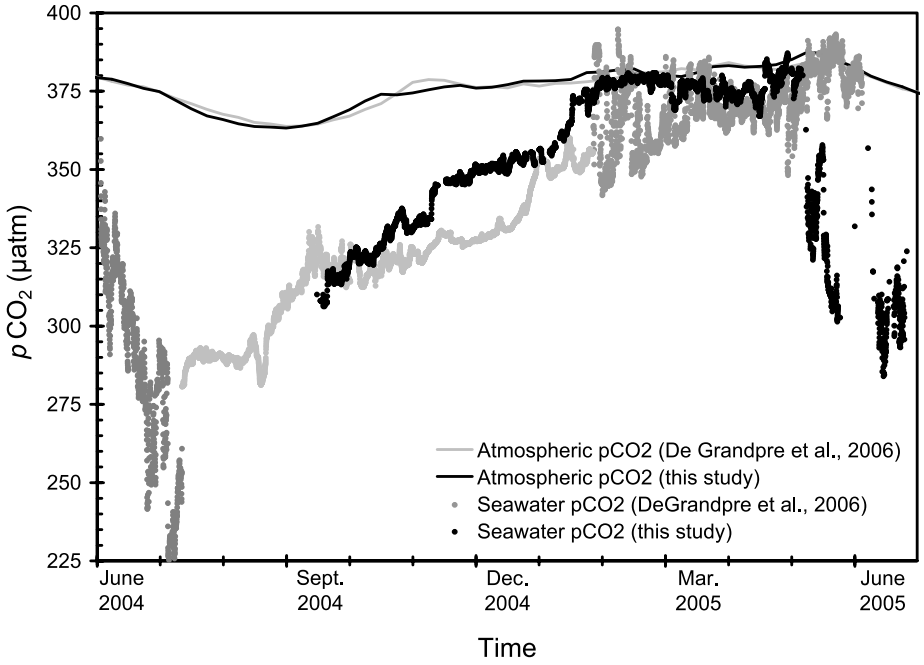

Figure 4. Comparison of pCO_2 time series at the K1 site from this study with a pilot study in 2000–2001 [*DeGrandpre et al.*, 2006] which combined mixed layer pCO_2 measurements (dark grey shade) with modeled pCO_2 data (light grey shade). The published earlier data were corrected upward by 8.0 μatm to account for the atmospheric CO_2 increase during this period.

the export production of the preceding spring/summer season which was respired above the base of the winter mixed layer. The net carbon drawdown observed during the spring bloom therefore does not represent the annual biological carbon sink from an atmospheric perspective. We will explore this in a more quantitative fashion in section 3.4.

[17] We compared our 2004–2005 data to the pCO_2 time series acquired during a pilot study in 2001–2002 [*DeGrandpre et al.*, 2006]. For this purpose the earlier data were adjusted upward by 8.0 μatm to account for the secular rise in atmospheric CO_2 concentrations that occurred over the 4 years separating the two times series (Figure 4). Note also that the time series of *DeGrandpre et al.* [2006] included the use of a one-dimensional biogeochemical model constrained by subsurface observations to estimate the surface pCO_2 time series for the period between 13 July 2000 and late January 2001 (indicated by the lighter shade of gray in Figure 4). Despite these adjustments and estimations the overall agreement between the two data sets is rather good. The earlier study captured the final stages of the 2000 spring bloom and the summer pCO_2 minimum very well. The (adjusted) minimum value of about 225 μatm in July–August 2000 is significantly lower, however, than the pCO_2 of about 285 μatm observed during the ship survey in July 2005. This could be due to interannual variability but we may also have simply missed the pCO_2 minimum in 2005. During late 2000–2001 winter, surface pCO_2 values also reached values at or near atmospheric equilibrium as was found for winter 2004–2005. Different from our study the onset of the spring bloom occurred about 3 weeks later in 2001 as compared to 2005.

[18] The seasonal O_2 cycle is shown in Figure 5. Here equilibrium with the atmosphere is reached in late summer/early fall when net community production has become small and the water column is still stratified. For some time (July–October) the various forcing factors for O_2 saturation, i.e., biogenic O_2 production and increasing O_2 solubility with seasonal cooling, appear either balanced or too weak to bring O_2 out of atmospheric equilibrium. This is only possible due to the roughly tenfold shorter-equilibration timescale of O_2 which is on the order of 1 month versus 1 year for CO_2. After October the O_2 supply from the atmosphere can no longer keep up with cooling and vertical mixing which entrains oxygen-deficient waters, and the mixed layer becomes undersaturated by about 8% in February 2005. The fact that oxygen levels remain at undersaturation around 6% (0–12%) throughout the winter period can be explained by the deeply mixed water column which represents a huge oxygen deficit that is in contact with the atmosphere through a comparatively small surface area (1 m^2 per 1000 m^3 of water at a convection depth of 1000 m). Enhanced variability toward the end of the winter season points at lateral exchange under strongly elevated eddy activity with some indication of a small early spring bloom around mid-April. The associated strong and rapid (hours) vertical movements of the sensor package during this period contribute a vertical signal that is not always fully removed by the filtering algorithm which is based on daily microwave SST data. The onset of the proper spring bloom is as evident as in pCO_2 with O_2 levels soaring up by about 50 μmol kg^{-1} to a supersaturation of up to 10%. Reequilibration for O_2 does not occur before July.

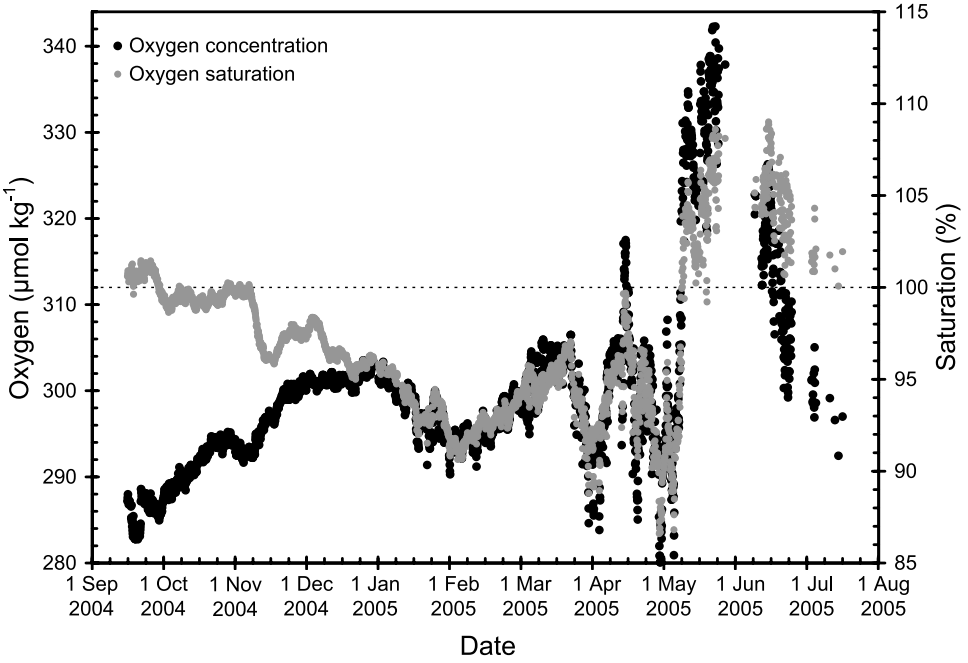

Figure 5. Mixed layer time series of oxygen concentration and saturation measured during the course of the K1 deployment. Oxygen saturation was calculated using the oxygen solubility after *Benson and Krause* [1984] at sea surface temperature, barometric pressure (Table 2), and 100% humidity.

[19] Overall, the observed seasonal cycles of CO_2 and O_2 agree rather well with the climatological situation as provided by *Takahashi et al.* [2002] for CO_2 and by *Najjar and Keeling* [1997, 2000] and *Keeling et al.* [1998] for O_2. For pCO_2 the peak-to-peak variation is very similar in data and climatology. It is obvious, however, that the space-time interpolation scheme involved in the construction of the pCO_2 climatology tends to smear out the sharp timing of the spring bloom (Figure 3). Our data show that the transition from the winter into the fully developed summer situation takes place in a matter of weeks, whereas the climatology shows a more gradual transition over 4 months. For O_2 the timing of the observed seasonal O_2 maximum in May 2005 is somewhat earlier than in the climatologies of *Najjar and Keeling* [1997] (i.e., 54–66°N zonal belt) and *Keeling et al.* [1998, Figure 1]. Also peak-to-peak variation in surface O_2 concentrations ($\sim$50 μmol kg^{-1}) is slightly larger than in the climatologies (35 and $\sim$40 μmol kg^{-1}, respectively). Similar to the situation for CO_2, the annual harmonics used in the O_2 climatologies cannot fully reproduce the sudden occurrence of the spring bloom and the full variability as well as the rapid changes associated with it.

3.2. Evaluation of Air-Sea Gas Exchange Parameterizations

[20] Net air-sea gas exchange can be calculated with a bulk equation which for CO_2 takes the following form:

$$F_{CO_2} = k_{CO_2} K_0 \left(pCO_2^{air} - pCO_2^{sea} \right). \quad (1)$$

Herein k_{CO2} is the transfer coefficient for CO_2, K_0 is the CO_2 solubility at in situ T and S after *Weiss* [1974], and pCO_2^{air} and pCO_2^{sea} are the CO_2 partial pressures (at 100% humidity and SST) of air and seawater, respectively.

[21] Similarly, O_2 flux densities can be calculated from equation (2) where k_{O2} is the transfer coefficient for O_2, and O_2^{sea} and O_2^{sat} are the measured and equilibrium O_2 concentrations of surface seawater, respectively. Here equilibrium O_2 concentrations O_2^{sat} were calculated at SST and barometric pressure (Table 2, 7-day running mean) using the solubility function of *Benson and Krause* [1984],

$$F_{O_2} = k_{O_2} \left(O_2^{sat} - O_2^{sea} \right). \quad (2)$$

[22] A variety of wind speed based parameterizations of the transfer coefficient k are available and the discussion about the best choice is still going on. We therefore explored the utility of our concomitant surface layer CO_2 and O_2 measurements to evaluate the most widely used parameterizations. We choose the following suite of parameterizations for short-term winds which essentially cover the full range and include linear, quadratic, and cubic wind speed dependencies: *Liss and Merlivat* [1986], *Wanninkhof* [1992], *Wanninkhof and McGillis* [1999], *Nightingale et al.* [2000], and *Sweeney et al.* [2007] (hereinafter referred to as LM86, W92, WM99, N2000, and S2007, respectively). Because of the strong nonlinearity of some of the parameterizations, transfer coefficients for CO_2 and O_2 were calculated on a 6-hour basis (rather than on the basis of weekly wind speed averages), thereby taking into account the observed wind speed distribution, and then averaged over the weekly calculation step. The resulting transfer coefficients were then scaled to observed SST using parameterizations of *Wanninkhof* [1992] for the temperature

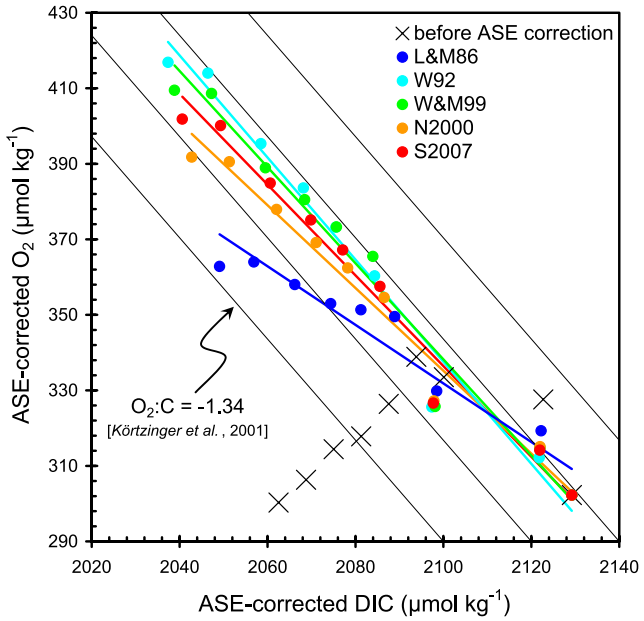

Figure 6. Correlation between mixed layer concentrations of DIC and O_2 before and after correction for the air-sea exchange component during a 9-week period in May–July 2005. Five different parameterizations for the gas transfer coefficient were used (see text for abbreviations). Also shown is the O_2:DIC relationship for biologically mediated changes with a stoichiometric O_2:C ratio of −1.34 [*Körtzinger et al.*, 2004].

dependence of the Schmidt numbers for CO_2 and O_2. By exploiting the tight stoichiometric constraint on biologically mediated DIC and O_2 changes we could test the validity of the various parameterizations.

[23] For the evaluation we tried to find a time period where (1) biologically mediated changes of DIC and O_2 were large, (2) as a consequence the CO_2 and O_2 disequilibria and hence the resulting fluxes were large too, and (3) the mixed layer was shallow so that changes in the DIC and O_2 inventories because of air-sea exchange and biological processes were also large. These criteria were only met during a 9-week period of the spring bloom (5 May to 7 July 2005) during which pCO_2 changed from near equilibrium to strong undersaturation and finally increasing pCO_2 levels toward the end while O_2 rose from strong undersaturation (∼10%) to strong supersaturation (∼10%) and near equilibrium toward the end. DIC was calculated from measured pCO_2 and climatological total alkalinity (Table 2) at in situ temperature and pressure using the CO2SYS software package [*Lewis and Wallace*, 1998] with the constants of *Mehrbach et al.* [1973] as refitted by *Dickson and Millero* [1987].

[24] O_2 release and CO_2 uptake during buildup and remineralization of organic matter in the ocean occur at a rather well-constrained O_2:C ratio. *Körtzinger et al.* [2001] found a value of −1.34 ± 0.06 for remineralization in the main thermocline. They were also able to show that the original value of −1.30 by *Redfield et al.* [1963] and the value of −1.45 ± 015 of *Anderson and Sarmiento* [1994] were at the upper and lower end of the biochemically plausible range. We therefore use the O_2:C ratio of −1.34 ± 0.06 by *Körtzinger et al.* [2001] as stoichiometric constraint. Because of the concomitant large impact of biological fluxes and air-sea exchange, mixed layer O_2 and DIC concentrations during the 9-week period did not vary in an instructive way (Figure 6). When corrected for the influence of air-sea exchange using the four different parameterizations, however, rather tight linear relationships were found in all cases. If advective signals are assumed to be absent, the observed slope should within error agree with the known stoichiometric O_2:C ratio of net community production if the influence of air-sea fluxes had been fully removed, i.e., if a valid air-sea exchange model had been used. Below we will explore to what degree this was the case with the five different parameterizations.

[25] The five slopes (Figure 6, Table 3) range from −0.78 to −1.36. Only when air-sea fluxes are corrected using the W92 and WM99 parameterizations the resulting slopes agree within error with the known stoichiometry. The agreement is borderline for the S2007 parameterization while air-sea fluxes estimated using the N2000 and especially the LM86 relationships are too weak to bring mixed layer O_2 and DIC values in line with the stoichiometric constraint. The wind speed measured every 6 hours during this period varied between 0.1 and 16.0 m s^{-1} with an average of 7.2 m s^{-1} (Figure 7). Interestingly, the transfer coefficients according to W92 and WM99 lie at the upper and lower end of the range (i.e., bracket the LM86, N2000, and S2007 estimates of k_{600}, the transfer coefficient for CO_2 in freshwater at 20°C) at wind speeds <8 m s^{-1}. At wind speed above about 10 m s^{-1}, however, W92 and WM99 yield transfer coefficients that are significantly higher than the other parameterization. The high wind speed range thus appears to be better represented by the stronger wind speed dependencies of W92 and WM99 causing the better agreement in this study.

[26] How does this reconcile with the results of *Sweeney et al.* [2007] who finally where able to close the gap between global-scale radiocarbon-based estimates and small-scale dual tracer studies by bringing down the bomb radiocarbon constraint by 25%? In the light of these findings the original bomb ^{14}C constrained W92 and WM99 parameterizations should overestimate gas exchange which is not what we found here. The fact, however, that the W92 and WM99 parameterizations disagree most (and bracket all other parameterizations) in the wind speed range <8 m s^{-1} indicates that it is not the lower end of the wind spectrum which causes the observed agreement or disagreement. In

Table 3. Observed O_2:DIC Slopes During 9-Week Spring Bloom Period After Correction of Mixed O_2 and DIC Concentrations for Net Air-Sea Fluxes of O_2 and CO_2, Respectively

Gas Exchange Parameterization	Resulting O_2:DIC Slope
Liss and Merlivat [1986]	−0.78 ± 0.10
Wanninkhof [1992]	−1.35 ± 0.06
Wanninkhof and McGillis [1999]	−1.27 ± 0.07
Nightingale et al. [2000]	−1.10 ± 0.06
Sweeney et al. [2007]	−1.20 ± 0.07

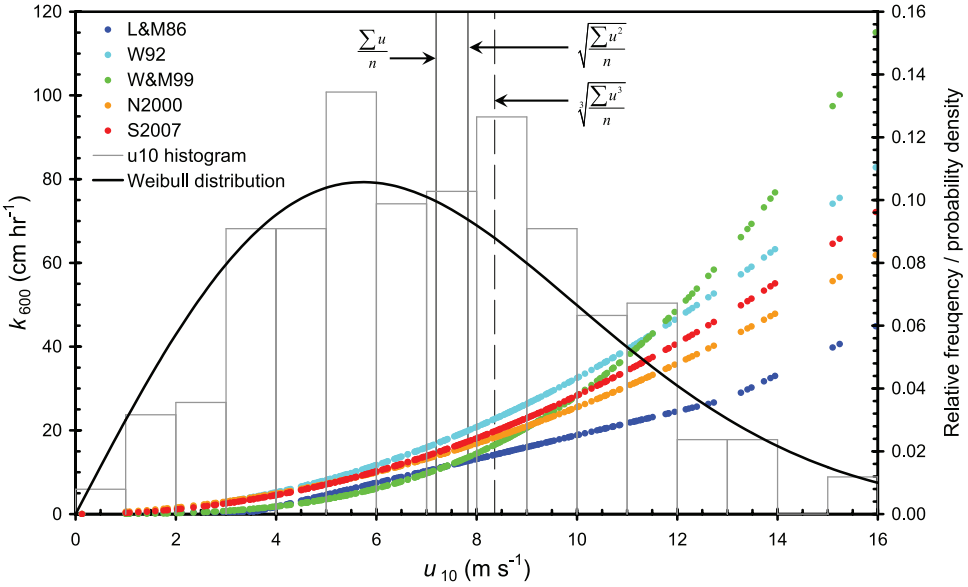

Figure 7. Transfer coefficients (normalized to a Schmidt number of 600) as calculated on the basis of wind speeds made every 6 hours during a 9-week period in May–July 2005 using five different parameterizations (see text for abbreviations). Also shown is a wind speed histogram as well as the probability distribution according to a Weibull function with a shape parameter $k = 2$.

contrast, it is the high wind speed range (>10 m s^{-1}) where both W92 and WM99 yield significantly higher transfer coefficient than the other three parameterizations. The bottom line of this is that the new radiocarbon constraint is not in contradiction with our findings, but the parameterization may require a stronger than quadratic wind speed dependency to accommodate the impact of higher wind speeds as seen in our results.

3.3. Air-Sea Fluxes of CO_2, O_2, and APO

[27] We calculated CO_2 and O_2 fluxes during the entire period using equations (1) and (2) and the parameterization of *Wanninkhof* [1992]. All computations are based on weekly averages of pCO_2^{air}, pCO_2^{sea}, O_2^{sat}, O_2^{sea}, k_{CO2}, k_{O2}, and SST. Equations (1) and (2) are defined such that fluxes of CO_2 or O_2 into the ocean are positive, that is, represent a gain of substance from the ocean's perspective. CO_2 fluxes (Figure 8a) are always directed into the ocean peaking during summer and nearly vanishing during winter when air-sea equilibrium is established. O_2 fluxes on the contrary change sign across the seasonal cycle from oceanic uptake during winter to outgassing in summer. Applying data from September 2004 also for September 2005, we were able to close the seasonal cycle and derive cumulative oceanic sinks of 2.7 ± 0.8 mol m^{-2} yr^{-1} (range, 2.0–2.9) for CO_2 and 10.0 ± 3.1 mol m^{-2} yr^{-1} (range, 7.7–11.2) for O_2. The error margin corresponds to the propagation of uncertainty in the pCO_2 ($\leq$10 μatm) and O_2 ($\leq$2 μmol L^{-1}) measurements. In addition, each flux estimate includes in brackets the flux range spanned by the WM99 (upper bound) and N2000 parameterizations (lower bound). Note that we did not calculate fluxes on the basis of LM86.

[28] Interestingly, the CO_2 sink is mostly driven by the spring/summer bloom and early winter periods of high wind speed whereas the O_2 sink occurs mostly during winter. The cumulative O_2 sink during the period of mixed layer deepening from end of October 2004 to early April 2005 amounts to 12.3 mol O_2 m^{-2} (range, 9.3–13.5) which is smaller than the value of *Körtzinger et al.* [2004] who estimated a buildup of the oxygen inventory during progressive mixed layer deepening of 17 mol O_2 m^{-2} in the preceding winter season, when the maximum convection depth was significantly deeper at ~1400 m. Outgassing of O_2 during the spring bloom offsets the winter influx by less than 20%.

[29] During recent years, concurrent measurements of CO_2 and O_2 in the atmosphere have been used successfully to separate the terrestrial and oceanic sinks of atmospheric CO_2 [e.g., *Keeling and Shertz*, 1992]. In an attempt to further exploit the information contained in atmospheric CO_2 and O_2 data, *Stephens et al.* [1998] defined a new tracer, atmospheric potential oxygen, which is a linear combination of atmospheric CO_2 and O_2 concentrations (APO = O_2 + 1.1 CO_2) that removes the terrestrial influence and most of the fossil fuel signal from atmospheric oxygen. Variations in APO therefore reflect mainly the air-sea exchange of O_2 and to a smaller extent also CO_2. Using our CO_2 and O_2 flux densities, we can calculate the APO flux density. Since APO is an atmospheric tracer, we use a different flux convention where oceanic uptake has a negative sign (i.e., a loss of matter from the atmosphere),

$$F_{APO} = -F_{O_2} - 1.1F_{CO_2}. \quad (3)$$

[30] As expected, the resulting APO flux densities (Figure 8b) are dominated by the O_2 fluxes. The annual flux of −13.0 ± 4.0 mol O_2 m^{-2} (range: −9.9– −14.3) mostly occurs in the winter season. During summer time the opposite

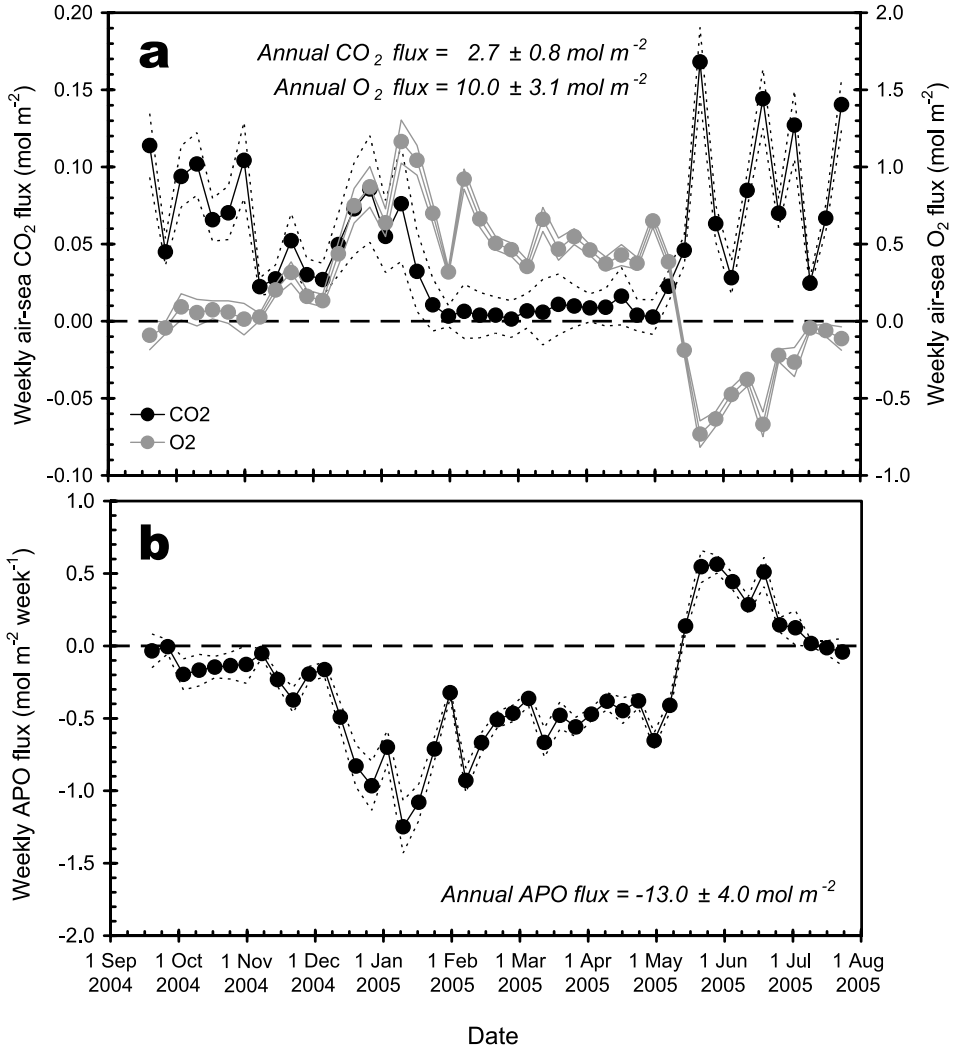

Figure 8. Weekly flux densities of (a) CO_2 and O_2 and (b) atmospheric potential oxygen (APO) at the K1 site during the course of the deployment. The error envelopes shown for each flux time series as well as the annual fluxes are a propagation of the maximum uncertainty in the pCO_2 ($\leq$10 μatm) and O_2 ($\leq$2 μmol L^{-1}) measurements. This error estimate does not include uncertainty associated with the choice among the available parameterizations of the transfer coefficient.

flux directions of CO_2 and O_2 partly compensate their APO influences with the oceanic uptake of CO_2 negating up to 25% of the oxygen-borne APO flux. The seasonal cycle of APO over the subpolar North Atlantic should therefore show a clear winter minimum and a rapid transition to the May–June summer maximum similar to what is observed at the atmospheric stations in Cold Bay, Alaska, USA (55.20°N, 162.72°W) or Sable Island, Nova Scotia, Canada (43.93°N, 60.02°W) [*Battle et al.*, 2006]. Unfortunately, no atmospheric site with high-quality measurements of CO_2 and O_2 exists downwind of the subpolar northwest Atlantic.

3.4. Physical and Biological Forcing of Surface Ocean pCO_2

[31] We follow a somewhat simplistic but nevertheless instructive way of separating thermal and biological (or more correctly nonthermal) forcing on the surface ocean pCO_2 that has previously been used by *Takahashi et al.* [2002]. This approach makes use of the fact that the temperature dependence of pCO_2 under isochemical conditions (i.e., fixed DIC and A_T) is well constrained ($\partial \ln pCO_2/\partial T$ = 0.04231°C^{-1}). This allows two measures: (1) construction of the thermally forced seasonal pCO_2 cycle ($pCO_{2,\mathrm{therm}}$, equation (4)) and (2) removal of the thermal effect from observed pCO_2 ($pCO_{2,\mathrm{nontherm}}$, equation (5)):

$$pCO_{2,\mathrm{therm}} = \overline{pCO_2} e^{0.0423\left(T_{\mathrm{obs}} - \overline{T}\right)} \tag{4}$$

$$pCO_{2,\mathrm{nontherm}} = pCO_{2,\mathrm{obs}} e^{0.0423\left(\overline{T} - T_{\mathrm{obs}}\right)}. \tag{5}$$

[32] Herein overbars denote annual means and obs stands for observed. Equation (4) perturbs the annual mean pCO_2 in surface seawaters at K1 (353.2 μatm) with the deviation

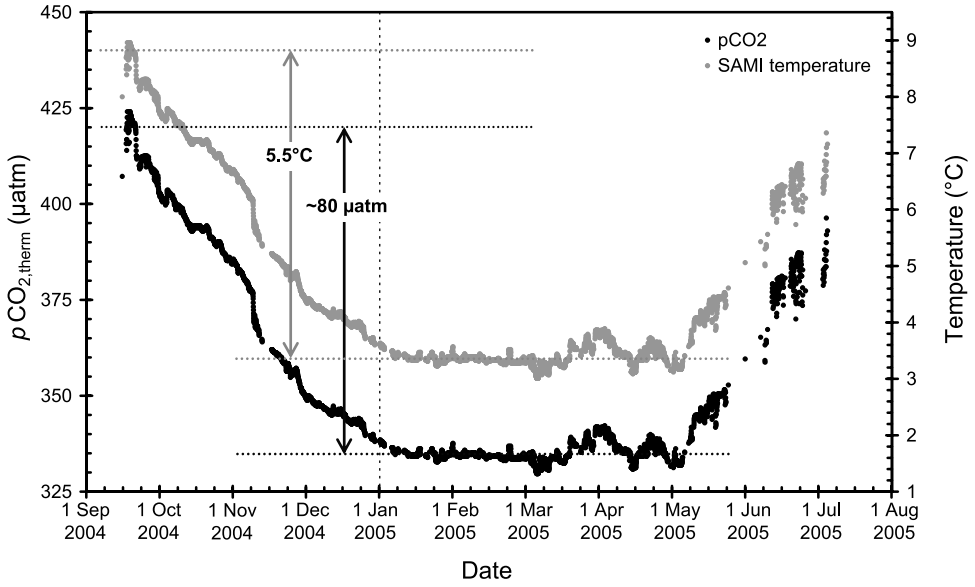

Figure 9. Perturbation of the mean pCO_2 during the observation period (353.2 μatm) with the deviation of observed SST from its annual mean. The resulting quantity $pCO_{2,therm}$ (equation (4)) is a measure of the (isochemical) thermal forcing of the seasonal pCO_2 cycle in the surface ocean.

of observed SST from its annual mean. The resulting $pCO_{2,therm}$ (Figure 9) can thus be looked at as the hypothetical pCO_2 that would be observed in an isochemical situation, i.e., no addition/removal of carbon by biological processes or air-sea exchange, which is characterized by the observed mean undersaturation. It is a realistic measure of the seasonal thermal forcing on surface ocean pCO_2. In contrast, equation (5) removes the thermal effect on the observed pCO_2 by correcting it to annual mean SST (5.96°C at the K1 site based on AMSR-E data from September 1, 2004 to August 31, 2005). The product $pCO_{2,nontherm}$ (Figure 10a) represents the observed pCO_2 variability that is not due to thermal effects and therefore must reflect chemical changes. These are biological carbon drawdown as well as DIC and/or A_T changes through advection, vertical entrainment, and diffusion as well as air-sea CO_2 exchange (DIC only).

[33] The seasonal peak-to-peak SST amplitude of ~5.5°C translates into a peak-to-peak variation of $pCO_{2,therm}$ of about 80 μatm (Figure 9). The summer-to-winter thermally driven pCO_2 decrease of 80 μatm is more than compensated by an increase of order 150 μatm due air-sea exchange and deepening of the mixed layer which brings CO_2 from wintertime DIC levels plus seasonal respiration back into the surface ocean (Figure 10b) causing the observed late winter maximum. Similarly, the winter-to-summer warming effect on pCO_2 is more than compensated by a counteractive consequence of net community production which explains the observed summer pCO_2 minimum.

[34] The seasonal DIC cycle (Figure 10b), as calculated from measured pCO_2 and climatological A_T (see section 3.2), shows a rapid decrease by >100 μmol kg^{-1} during the spring bloom. The onset of the bloom, however, occurred well past the onset of stratification and is therefore restricted to a shallow mixed layer. Entrainment by definition must be zero under conditions of stationary mixed layer depths. We furthermore assume that the diffusive flux is negligible in this context. The masking effect of uptake of atmospheric CO_2 on the biologically mediated DIC change can be calculated explicitly and removed. In contrast, the role of advection is generally more critical and cannot be corrected for easily.

[35] We therefore explored current velocities measured by current meters deployed at depths of 164, 308, and 1509 m in the same mooring (Figure 11a). These show high barotropicity and can therefore be used to infer advection at the sensor depth of ~38 m. The 164-m currents were separated into northward and eastward components and binned into 7-day averages (Figure 11b) which show rather low-advection activity until the end of March 2004 with average scalar current speeds of ~0.05 m s^{-1} that correspond to advection length scales of ~30 km week^{-1} (or ~130 km month^{-1}). This is typical for the station's setting in the center of the deep convection region in the central Labrador Sea gyre. In fact, the mooring location had been chosen such that lateral signals would be small compared to the strong seasonal cycle of vertical mixing. In April the region is characterized by the crossing of a tongue of elevated eddy kinetic energy (EKE) which represents a marked maximum of the annual EKE cycle at K1 [*Lilly et al.*, 2003; *Brandt et al.*, 2004]. As we will show later this short period of strongly enhanced EKE coincides with, and may in fact be instrumental in, the triggering of the spring bloom. After this, peak advection activity is strongly reduced although the presence of mesoscale eddies is still visible. During the May–July period of strong carbon drawdown the average scalar current speed is 0.09 m s^{-1}. At advection length scales of ~50 km week^{-1} and a general southward flow direction we are confident that the observed temporal changes are representative of the central and

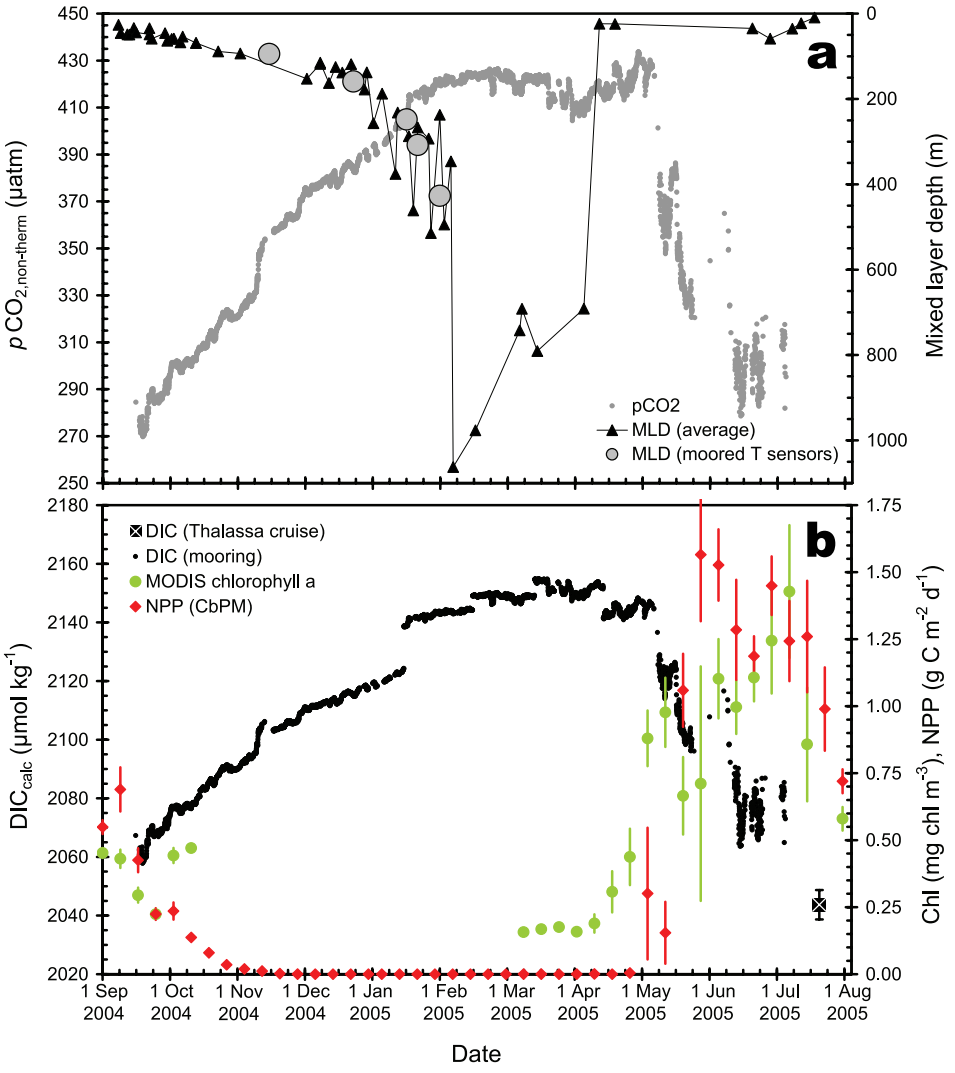

Figure 10. (a) Observed pCO_2 corrected to the annual mean SST (5.96°C based on AMSR-E data from September 1, 2004 to August 31, 2005). The resulting quantity $pCO_{2,nontherm}$ (equation (5)) is a measure of the chemically driven (isothermal) pCO_2 cycle in the surface ocean. Figure 10a also includes estimated mixed layer depths. (b) Mixed layer time series of dissolved inorganic carbon concentrations (DIC), calculated from observed pCO_2 and climatological total alkalinity (Table 2). Also shown for the K1 site are remotely sensed chlorophyll *a* concentrations from the Moderate Resolution Imaging Spectroradiometer sensor (NASA Aqua satellite, 8-day averages of 16 pixels from the 1080 × 2160 global grid) as well as net primary production estimates (CBPM, 8-day averages of 6 pixels from the 540 × 1080 global grid).

supposedly rather homogenous Labrador Sea convection region. Given the strength and direction of the flow field a significant influence from the boundary current can be ruled out.

[36] During this bloom period (mid-May to the third week of July) we found an integrated carbon drawdown (equal to net community production (NCP)) of 4.0 ± 0.8 mol C m^{-2} (=48 g C m^{-2}) in the shallow mixed layer. We compared this to net primary production (NPP) estimated using two prominent methods: (1) remotely sensed chlorophyll concentrations and a light-dependent, depth-resolved model for carbon fixation (Vertically Generalized Production Model (VGPM) [*Behrenfeld and Falkowski*, 1997]) and (2) a new approach based on remotely sensed chlorophyll concentrations and particulate backscattering coefficients (Carbon-Based Production Model (CBPM) [*Behrenfeld et al.*, 2006]). The two methods, which use the same chlorophyll data and parameterizations for the light dependence and euphotic depth, yield similar NPP values of 7.7 mol C m^{-2} (VGPM) and 8.0 mol C m^{-2} (CBPM) during the period from mid-May to the third week of July 2005. The comparison shows high synchronicity between carbon drawdown and the estimated NPP (Figure 10b). A quantitative comparison of NCP and NPP is not feasible as the former by necessity is restricted to the mixed layer while the latter is calculated across the photic zone. In the prevailing

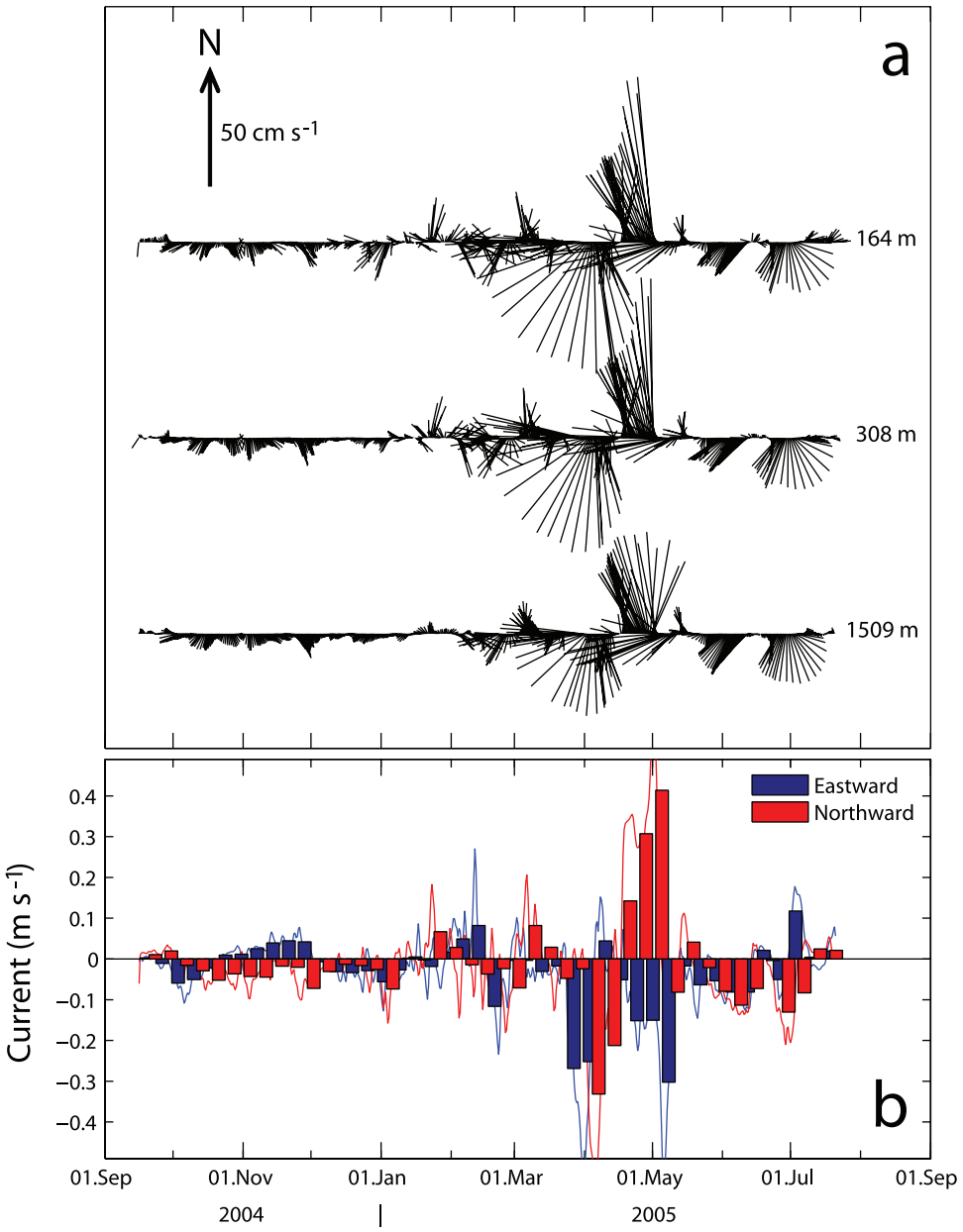

Figure 11. Current measurements during the 2004–2005 deployment at the K1 site: (a) stick vectors at three depths and (b) northward and eastward current speed with 7-day averages at 164 m depth.

situation of shallow mixing NPP that occurs below the mixed layer is not mirrored in our NCP estimate.

[37] We assume that most of the seasonal NCP is exported out of the mixed layer (as opposed to accumulation within it). Some of this material will undergo remineralization above the base of the winter mixed layer and the evolving respiratory CO_2 can thus be ventilated back to the surface ocean during the following winter. A simple budget calculation assuming repetition of the observed seasonal DIC cycle in the following 2005–2006 winter season and using mixed layer conditions at the end of deep mixing in March–April 2005 as well as the end of the productive season in late July 2005 yields a reflux of 1.4 ± 0.5 mol C m^{-2} of respiratory CO_2 back into the surface mixed layer. This accounts for about one third of the seasonal NCP of 4.0 ± 0.8 mol C m^{-2} and leaves about 2.6 ± 1.3 mol C m^{-2} yr^{-1} which must have been exported to below the base of the winter mixed layer.

[38] The estimated seasonal NCP of 4.0 mol C m^{-2} is only about 60% of the seasonal NCP found by *Körtzinger et al.* [2008] for the northeast Atlantic Ocean (49°N, 16.5°W) where wintertime nutrients levels are comparable. The major reason for this difference appears to be the different timing of the spring bloom which starts well in advance of

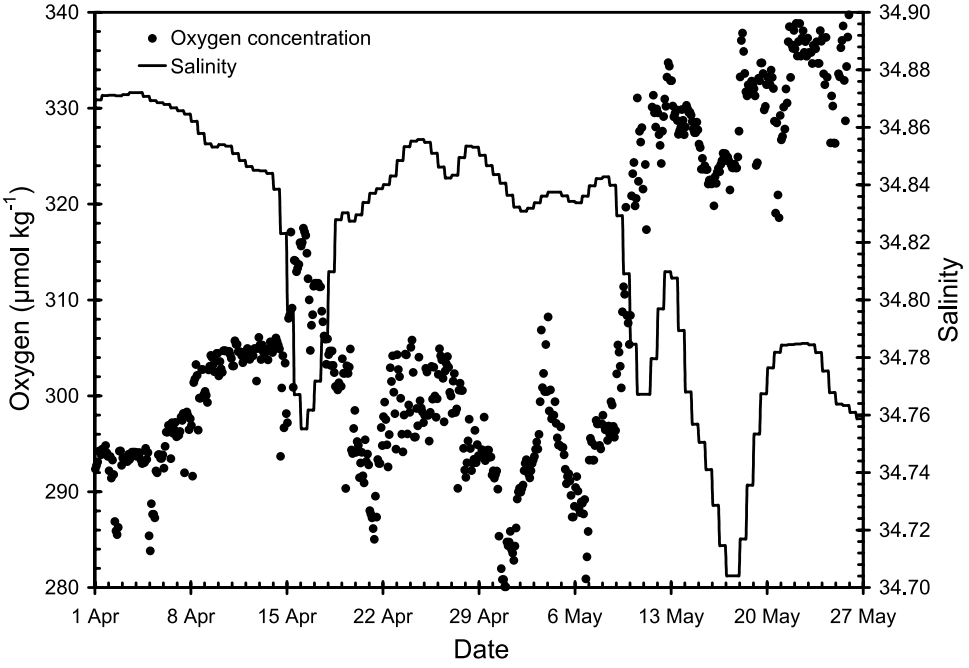

Figure 12. Observed oxygen concentration and salinity during the weeks before and after the onset of the spring bloom in early May 2005 highlighting the coincidence of fresher surface waters with higher-oxygen concentrations.

stratification in the northeast Atlantic and therefore, at similar nutrient concentrations, taps on a much larger nutrient reservoir in the mixed layer. At K1 in the Labrador Sea the available nutrient reservoir is already restricted to a very shallow summer mixed layer when the spring bloom starts. The timing of the bloom as evident in the CO_2 and O_2 data agrees very well with the sudden occurrence of enhanced chlorophyll levels as seen by the Moderate Resolution Imaging Spectroradiometer (MODIS) on the NASA Aqua satellite (Figure 10b). Similarly, the increase, peak, and decline of the CBPM NPP estimates (Figure 10b, 8-day averages of six pixels from the 540 × 1080 global grid) coincide very well with the chemical signatures observed during this study.

[39] It is an interesting question what might trigger the late spring bloom at the K1 site. There is no evidence that stratification itself plays an important role in the triggering of bloom. Solar irradiance is certainly a key variable but cannot explain the sharp onset of the spring bloom in May. It is noteworthy that the proper spring bloom, but also a brief transient period of elevated oxygen levels in the middle of April, coincide with negative spikes in the salinity record (Figure 12). The latter are most likely associated with eddies that spin off the West Greenland Current because of barotropic instability generated near Cape Desolation [*Eden and Böning*, 2002; *Brandt et al.*, 2004; *Hátún et al.*, 2007]. The regional EKE maximum in March–April [*Lilly et al.*, 2003; *Brandt et al.*, 2004] is clearly visible in the current record at K1 (Figure 11) which basically shows the passage of a single intense eddy the core of which passed around mid-April, i.e., exactly when the low-salinity and high-oxygen patterns were observed (Figure 12).

[40] The eddy structures that were accompanied by elevated productivity in our observations are fresher than surrounding waters which points to their origin in the polar waters of the West Greenland Current. Such buoyant, anticyclonic eddies with low-salinity cores above 200 m have indeed been observed recently [*Hátún et al.*, 2007] and appear to be important for rapid restratification of the Labrador Sea after winter convection. As we show here, they may also play a vital role in the triggering of the surface bloom in the central Labrador Sea. Our data provide no further insight into the driving mechanism(s), and we can only speculate that these fresher waters deliver an essential component such as iron necessary to alleviate a hypothetical iron limitation or a phytoplankton seed population from a neighboring biogeochemical province, the Boreal Polar Province, which thrives in a region that biogeographically is characterized by a dominance of Atlantic species [*Longhurst*, 2007].

4. Conclusions

[41] In this paper we present the first highly resolved annual cycles of pCO_2 and O_2 measured in the central Labrador Sea. The region is one of the few places in the world ocean where deep convection takes place during winter time. It further hosts sizable biological productivity confined to a short spring/summer period. On the basis of our analyses of the seasonal pCO_2 and O_2 cycles we can draw the following conclusions:

[42] 1. The seasonal pCO_2 cycle in the Labrador Sea is characterized by a marked summer minimum (winter maximum). The effect of summertime biological carbon drawdown on pCO_2 exceeds the counteractive effect of the seasonal SST cycle (hence the summer pCO_2 minimum). Close agreement with the climatological pCO_2 was found, with the exception that the sharp onset of the spring bloom is blurred in the climatology.

[43] 2. The central Labrador Sea acts as a sink for atmospheric CO_2. In 2004–2005 we estimated a CO_2 uptake of about 2.7 ± 0.8 mol m^{-2} yr^{-1} which is 15% less than the climatological flux of 3.2 mol m^{-2} yr^{-1} for the pixel centered at 56°N, 52.5°W [*Takahashi et al.*, 2002] and 40% less than the estimate of *DeGrandpre et al.* [2006] for annual cycle 2000–2001. The observed CO_2 sink is mostly mediated by biological productivity during the summer period. During wintertime, surface seawater pCO_2 approaches atmospheric equilibrium as the effects of deep convection (reventilation of respiratory CO_2 that stems from a sizable fraction of the summertime biological carbon export) counteracts the cooling effect on surface pCO_2. During colder and hence more convective years, more respiration CO_2 will be entrained into the surface mixed layer that counteracts the effect of stronger cooling. Also stronger vertical entrainment of DIC (along with nutrients) should lead to enhanced net productivity in the next productive season. In contrast to oxygen these counteractive effects cause a damping of interannual variability in the net CO_2 sink [*McKinley et al.*, 2004].

[44] 3. The seasonal O_2 cycle features a marked period of undersaturation by around 6% during winter time when large volumes of oxygen-deficient waters are ventilated to the atmosphere. The brief period of supersaturation by up to 10% during spring/summer is driven by the phytoplankton that is confined to a rather shallow mixed layer.

[45] 4. The central Labrador Sea also acts as a sink for atmospheric oxygen. During our 2004–2005 observation period we estimated an annual O_2 sink of about 10.0 ± 3.1 mol m^{-2} yr^{-1}. The large O_2 uptake of 12.3 mol m^{-2} that occurs during the period of mixed layer deepening between October and April is partly offset by an O_2 source during the productive spring/summer season. This dominant role of deep convection supports the existence of a link between interannual variability in convection activity in the Labrador Sea [*Avsic et al.*, 2006] and interannual variability of air-sea O_2 fluxes [*McKinley et al.*, 2004].

[46] 5. In the Labrador Sea, annual CO_2 and O_2 fluxes are in the same direction and therefore reinforce each other in their influence on atmospheric potential oxygen. At an estimated APO flux of -13.0 ± 4.0 mol O_2 yr^{-1} the region should exert a noticeable imprint on regional APO patterns.

[47] 6. A mixed layer budget yielded a net community production (NCP) during the spring/summer bloom of 4.0 mol C m^{-2} the timing of which agrees very well with the timing of the net primary production during this period (7.7–8.0 mol C m^{-2}) as estimated from remotely sensed products. A rough estimate indicates that about one third of the NCP is respired above the base of the winter mixed layer and returned to the atmosphere during the following convective season.

[48] 7. The surface ocean system shows a dramatic and rapid change from deep winter mixing to shallow summer stratification. This transition does not trigger, however, the onset of the spring bloom which occurred more than 1 month later in summer 2005. In contrast, enhanced productivity appears to be associated with lower salinity which is indicative of eddies importing waters of polar origin from the West Greenland Current that may bring in an essential component such as bioavailable iron or a phytoplankton seed population.

[49] 8. The parameterizations of the air-sea gas transfer coefficient by *Wanninkhof* [1992] and *Wanninkhof and McGillis* [1999] were found to be in best agreement with the observed mixed layer dynamics of CO_2 and O_2 during the spring bloom period. This points at a strong wind dependence at high wind speed (>10 m s^{-1}).

[50] **Acknowledgments.** We would like to acknowledge the efforts and skills of the ship crews and scientific parties which prepared, deployed, recovered, and refurbished the multidisciplinary K1 mooring. We thank Cory Beatty (Department of Chemistry, University of Montana, Missoula, United States) for quality checks of the SAMI pCO_2 data. We also thank Robert O'Malley (Department of Botany and Plant Pathology, Oregon State University, Corvallis, Oregon, United States) for providing the VGPM and CBPM productivity estimates as well as MODIS chlorophyll data for the K1 site. Finally, we are grateful to two anonymous reviewers who helped to improve the manuscript. This paper was written during a sabbatical of the first author (A.K.) at the School of Oceanography, University of Washington, Seattle, United States, for which he is particularly grateful to his host Paul Quay. The present work was funded by the Collaborative Research Centre 460 (SFB 460) of the German Research Foundation.

References

Anderson, L. A., and J. L. Sarmiento (1994), Redfield ratios of remineralization determined by nutrient data analysis, *Global Biogeochem. Cycles*, *8*, 65–80.

Avsic, T., J. Karstensen, U. Send, and J. Fischer (2006), Interannual variability of newly formed Labrador Sea Water from 1994 to 2005, *Geophys. Res. Lett.*, *33*, L21S02, doi:10.1029/2006GL026913.

Battle, M., et al. (2006), Atmospheric potential oxygen: New observations and their implications for some atmospheric and oceanic models, *Global Biogeochem. Cycles*, *20*, GB1010, doi:10.1029/2005GB002534.

Behrenfeld, M. J., and P. G. Falkowski (1997), Photosynthetic rates derived from satellite-based chlorophyll concentration, *Limnol. Oceanogr.*, *42*, 1–20.

Behrenfeld, M. J., R. T. O'Malley, D. A. Siegel, C. R. McClain, J. L. Sarmiento, G. C. Feldman, A. J. Milligan, P. G. Falkowski, R. M. Letelier, and E. S. Boss (2006), Climate-driven trends in contemporary ocean productivity, *Nature*, *444*, 752–755.

Benson, B. B., and D. Krause Jr. (1984), The concentration and isotopic fractionation of oxygen dissolved in freshwater and seawater at equilibrium with the atmosphere, *Limnol. Oceanogr.*, *29*, 620–632.

Brandt, P., F. A. Schott, A. Funk, and C. S. Martins (2004), Seasonal to interannual variability of the eddy field in the Labrador Sea from satellite altimetry, *J. Geophys. Res.*, *109*, C02028, doi:10.1029/2002JC001551.

de Boyer Montégut, C., G. Madec, A. S. Fischer, A. Lazar, and D. Iudicone (2004), Mixed layer depth over the global ocean: An examination of profile data and a profile-based climatology, *J. Geophys. Res.*, *109*, C12003, doi:10.1029/2004JC002378.

DeGrandpre, M. D., T. R. Hammar, S. P. Smith, and F. L. Sayles (1995), In situ measurements of seawater pCO_2, *Limnol. Oceanogr.*, *40*, 969–975.

DeGrandpre, M. D., M. M. Baehr, and T. R. Hammar (1999), Calibration-free optical chemical sensors, *Anal. Chem.*, *71*, 1152–1159.

DeGrandpre, M. D., A. Körtzinger, U. Send, D. W. R. Wallace, and R. G. J. Bellerby (2006), Uptake and sequestration of atmospheric CO_2 in the Labrador Sea deep convection region, *Geophys. Res. Lett.*, *33*, L21S03, doi:10.1029/2006GL026881.

Dickson, A. G., and F. J. Millero (1987), A comparison of the equilibrium constants for the dissociation constants of carbonic acid in seawater media, *Deep Sea Res.*, *34*, 1733–1743.

Dickson, B., I. Yashayaev, J. Meincke, B. Turrell, S. Dye, and J. Holfort (2002), Rapid freshening of the deep North Atlantic Ocean over the past four decades, *Nature*, *416*, 832–837.

Eden, C., and C. Böning (2002), Sources of eddy kinetic energy in the Labrador Sea, *J. Phys. Oceanogr.*, *32*, 3346–3363.

Emery, W. J., P. Brandt, A. Funk, and C. Böning (2006), A comparison of sea surface temperatures from microwave remote sensing of the Labrador Sea with in situ measurements and model simulations, *J. Geophys. Res.*, *111*, C12013, doi:10.1029/2006JC003578.

Garcia, H. E., and R. F. Keeling (2001), On the global oxygen anomaly and air-sea flux, *J. Geophys. Res.*, *106*(C12), 31,155–31,166.

Hátún, H., C. C. Eriksen, and P. B. Rhines (2007), Buoyant eddies entering the Labrador Sea observed with gliders and altimetry, *J. Phys. Oceanogr.*, *37*, 2838–2854.

Keeling, R. F., and S. R. Shertz (1992), Seasonal and interannual variations in atmospheric oxygen and implications for the global carbon cycle, *Nature*, *358*, 723–727.

Keeling, R. F., B. B. Stephens, R. G. Najjar, S. C. Doney, D. Archer, and M. Heimann (1998), Seasonal variations in the atmospheric O_2/N_2 ratio in relation to the kinetics of air-sea gas exchange, *Global Biogeochem. Cycles*, *12*(1), 141–164.

Körtzinger, A., J. I. Hedges, and P. D. Quay (2001), Redfield ratios revisited: Removing the biasing effect of anthropogenic CO_2, *Limnol. Oceanogr.*, *46*, 964–970.

Körtzinger, A., J. Schimanski, U. Send, and D. W. R. Wallace (2004), The ocean takes a deep breath, *Science*, *306*, 1337.

Körtzinger, A., J. Schimanski, and U. Send (2005), High-quality oxygen measurements from profiling floats: A promising new technique, *J. Atmos. Oceanic Technol.*, *22*, 302–308.

Körtzinger, A., U. Send, R. S. Lampitt, S. Hartman, D. W. R. Wallace, J. Karstensen, M. G. Villagarcia, O. Llinas, and M. D. DeGrandpre (2008), Seasonal pCO_2 cycle at 49°N/16.5°W in the northeast Atlantic Ocean and what it tells us about biological productivity, *J. Geophys. Res.*, doi:10.1029/2007JC004347, in press.

Lazier, J., R. Hendry, A. Clarke, I. Yashayaev, and P. Rhines (2002), Convection and restratification in the Labrador Sea, 1990–2000, *Deep Sea Res. Part I*, *49*, 1819–1835.

Lee, K., L. T. Tong, F. J. Millero, C. L. Sabine, A. G. Dickson, C. Goyet, G.-H. Park, R. Wanninkhof, R. A. Feely, and R. M. Key (2006), Global relationships of total alkalinity with salinity and temperature in surface waters of the world's oceans, *Geophys. Res. Lett.*, *33*, L19605, doi:10.1029/2006GL027207.

Lefèvre, N., A. J. Watson, A. Olsen, A. F. Ríos, F. F. Pérez, and T. Johannessen (2004), A decrease in the sink for atmospheric CO_2 in the North Atlantic, *Geophys. Res. Lett.*, *31*, L07306, doi:10.1029/2003GL018957.

Levitus, S., J. Antonov, and T. Boyer (2005), Warming of the world ocean, 1955–2003, *Geophys. Res. Lett.*, *32*, L02604, doi:10.1029/2004GL021592.

Lewis, E., and D. W. R. Wallace (1998), Program Developed for CO_2 System Calculations, *ORNL/CDIAC-105*, Carbon Dioxide Inf. Anal. Cent., Oak Ridge Natl. Lab., U.S. Dep. of Energy, Oak Ridge, Tenn.

Lilly, J. M., P. B. Rhines, F. Schott, K. Lavender, J. Lazier, U. Send, and E. D'Asaro (2003), Observations of the Labrador Sea eddy field, *Prog. Oceanogr.*, *59*, 75–176.

Liss, P. S., and L. Merlivat (1986), Air-sea gas exchange rates: Introduction and synthesis, in *The Role of Air-Sea Exchange in Geochemical Cycling*, edited by P. Buat-Ménard, pp. 113–127, D. Reidel, Dordrecht, Netherlands.

Longhurst, A. R. (2007), *Ecological Geography of the Sea*, 2nd ed., 542 pp., Academic, Amsterdam.

Lüger, H., D. W. R. Wallace, A. Körtzinger, and Y. Nojiri (2004), The pCO_2 variability in the midlatitude North Atlantic Ocean during a full annual cycle, *Global Biogeochem. Cycles*, *18*, GB3023, doi:10.1029/2003GB002200.

McKinley, G. A., M. J. Follows, and J. Marshall (2004), Mechanisms of air-sea CO_2 flux variability in the equatorial Pacific and the North Atlantic, *Global Biogeochem. Cycles*, *18*, GB2011, doi:10.1029/2003GB002179.

Mehrbach, C., C. H. Culberson, J. E. Hawley, and R. M. Pytkowicz (1973), Measurement of the apparent dissociation constants of carbonic acid in seawater at atmospheric pressure, *Limnol. Oceanogr.*, *18*, 897–907.

Monterey, G., and S. Levitus (1997), Seasonal variability of mixed layer depth for the World Ocean, *NOAA NESDIS Atlas 14*, 100 pp., Natl. Oceanic and Atmos.c Admin., Washington, D.C.

Najjar, R. G., and R. F. Keeling (1997), Analysis of the mean annual cycle of the dissolved oxygen anomaly in the World Ocean, *J. Mar. Res.*, *55*, 117–151.

Najjar, R. G., and R. F. Keeling (2000), Mean annual cycle of the air-sea oxygen flux: A global view, *Global Biogeochem. Cycles*, *14*(2), 573–584.

Nightingale, P. D., G. Malin, C. S. Law, A. J. Watson, P. S. Liss, M. I. Liddicoat, J. Boutin, and R. C. Upstill-Goddard (2000), In situ evaluation of air-sea gas exchange parameterizations using novel conservative and volatile tracers, *Global Biogeochem. Cycles*, *14*(1), 373–388.

Omar, A. M., and A. Olsen (2006), Reconstructing the time history of the air-sea CO_2 disequilibrium and its rate of change in the eastern subpolar North Atlantic, 1972–1989, *Geophys. Res. Lett.*, *33*, L04602, doi:10.1029/2005GL025425.

Redfield, A. C., B. H. Ketchum, and F. A. Richards (1963), The influence of organisms on the composition of sea water, in *The Sea*, edited by M. N. Hill, pp. 26–77, Interscience, New York.

Stephens, B. B., R. F. Keeling, M. Heimann, K. D. Six, R. Murnane, and K. Caldeira (1998), Testing global ocean carbon cycle models using measurements of atmospheric O_2 and CO_2 concentration, *Global Biogeochem. Cycles*, *12*, 213–230.

Sweeney, C., E. Gloor, A. R. Jacobson, R. M. Key, G. McKinley, J. L. Sarmiento, and R. Wanninkhof (2007), Constraining global air-sea gas exchange for CO_2 with recent bomb ^{14}C measurements, *Global Biogeochem. Cycles*, *21*, GB2015, doi:10.1029/2006GB002784.

Takahashi, T., J. Olafsson, J. Goddard, D. W. Chipman, and S. C. Sutherland (1993), Seasonal variation of CO_2 and nutrients in the high-latitude surface oceans: A comparative study, *Global Biogeochem. Cycles*, *7*, 843–878.

Takahashi, T., et al. (2002), Global air-sea CO_2 flux based on climatological surface ocean pCO_2, and seasonal biological and temperature effects, *Deep Sea Res. Part II*, *49*, 1601–1622.

Tengberg, A., et al. (2006), Evaluation of a life time based optode to measure oxygen in aquatic systems, *Limnol. Oceanogr. Methods*, *4*, 7–17.

Wanninkhof, R. (1992), Relationship between wind speed and gas exchange over the ocean, *J. Geophys. Res.*, *97*, 7373–7382.

Wanninkhof, R., and W. R. McGillis (1999), A cubic relationship between air-sea CO_2 exchange and wind speed, *Geophys. Res. Lett.*, *26*, 1889–1892.

Weiss, R. F. (1974), Carbon dioxide in water and seawater: The solubility of a non-ideal gas, *Mar. Chem.*, *2*, 203–215.

Wentz, F., and T. Meissner (2004), AMSR-E/Aqua Daily L3 Global Ascending/Descending 0.25° × 0.25° Ocean Grids V001, March to June 2004, http://www-nsidc.colorado.edu/data/amsre/data_summaries.html, Natl. Snow and Ice Data Center, Boulder, Colo.

M. DeGrandpre, Department of Chemistry, University of Montana, 32 Campus Drive, Missoula, MT 59812, USA.

J. Karstensen, Leibniz Institute of Marine Sciences, Physical Oceanography, University of Kiel, East Shore Campus, Wischhofstr. 1-3, D-24148 Kiel, Germany.

A. Körtzinger and D. W. R. Wallace, Leibniz Institute of Marine Sciences, Chemical Oceanography, University of Kiel, East Shore Campus, Wischhofstr. 1-3, D-24148 Kiel, Germany. (akoertzinger@ifm-geomar.de)

U. Send, Scripps Institution of Oceanography, University of California at San Diego, 8602 La Jolla Shores Drive, La Jolla, CA 92037, USA.